International Journal of Thermal Sciences 183 (2023) 107858

Contents lists available at ScienceDirect

International Journal of Thermal Sciences

journal homepage: www.elsevier.com/locate/ijts

Collective effects during the formation of child droplets as a result of puffing/micro-explosion of composite droplets

D.V. Antonov, R.M. Fedorenko, P.A. Strizhak *

National Research Tomsk Polytechnic University, Heat Mass Transfer Laboratory, 30 Lenin Avenue, Tomsk, 634050, Russia

ARTICLE INFO

Keywords:
Group of droplets
Water/diesel blends
Micro-explosion
Puffing
Child droplets
Collective effects

ABSTRACT

Puffing and micro-explosion are among the major phenomena behind the industrial secondary atomization of composite droplets. These effects significantly reduce the average size of secondary droplets formed during the jet breakup to 5–10 times of the original droplet size in the case of puffing and to 100–200 times in the case of micro-explosion. The initial droplet sizes (radii) ranged from 0.5 to 1.5 mm. Here we present the research findings on the collective effects during the formation of child droplets as a result of puffing/micro-explosion of composite droplets. We have analyzed the characteristics of child droplets formed during the micro-explosive fragmentation of a group of three composite droplets. We used two fuel blends: 90 vol% of Diesel fuel, 10 vol % of water; 10 vol% of Diesel fuel, 90 vol% of water. Typical sizes of child droplets formed during the fragmentation of each droplet in a group were determined by shadowgraphy. The number and size of secondary fragments practically do not change when the distances between parent droplets do not exceed 8–10 radii. In these conditions, the integral fragmentation characteristics of a group of droplets are in acceptable agreement with those of isolated droplets. With shorter distances between droplets, there are considerable differences in the characteristics of secondary droplets formed during the puffing/micro-explosion of composite droplets. Conditions were recorded in which puffing or micro-explosion can occur as a result of collisions between secondary fragments and parent droplets.

1. Introduction

Secondary atomization of droplets (in the partial or full fragmentation regime) in multi-phase and multi-component fuel flows is a promising technology that can minimize fuel consumption, improve the combustion dynamics, reduce anthropogenic emissions, stabilize fuel injection in a combustion chamber, and reduce the equipment wear [1–3]. The most promising secondary atomization schemes involve droplet-droplet collisions in intersecting fuel jets [4], droplet collisions with a solid surface in the form of walls, rings, meshes, and ledges [5], micro-explosion and puffing [6–8]. As a result of a micro-explosion, droplets of multi-phase and multi-component fuels break up to form an array of liquid fragments with a size of 1–100 μm [1]. This allows for a manyfold increase in the evaporation surface area in a combustion chamber. With this in mind, obtaining fine mist through micro-explosion is the optimal choice in terms saving both time and energy on droplet heating to breakup. At first, researchers focused on the conditions of micro-explosion as well as internal and external parameters that affect these conditions. The main reason for the occurrence of puffing and micro-explosion was found to be the superheating of the less volatile component (water) near the water/fuel interface above the boiling (nucleation) point [9]. No less important is the research into breakup outcomes of composite droplets (for instance, the size of child droplets and the mist cloud incorporating them). In order to ensure the optimal operation of engineering and process equipment, it is necessary to find the conditions necessary for the formation of child droplets with specific sizes and velocities [2,10,11]. The breakup behavior of composite droplets depends on a number of factors. For instance, the sizes and velocities of child droplets—and hence their momentum—depend on the size of the dispersed phase in emulsions (micro-droplets of water in a drop of Diesel fuel or another combustible liquid). Most of the droplet size distributions obtained in the experiments are near-normal [12]. Refs. [6,7] focus on thermal, kinetic, and surface energy of child droplets. Tarlet et al. [6] suggest that the thermal energy distributions as a function of the number of emerging child droplets are log-normal. The distributions of the secondary fragments'

* Corresponding author.
E-mail address: pavelspa@tpu.ru (P.A. Strizhak).
URL: http://hmtslab.tpu.ru/ (P.A. Strizhak).

https://doi.org/10.1016/j.ijthermalsci.2022.107858
Received 8 July 2022; Received in revised form 1 August 2022; Accepted 9 August 2022

kinetic energy are established in Ref. [7] and their log-normal distribution is suggested. The breakup behavior of W/D (water/Diesel) emulsion droplets is significantly affected by the size of the dispersed phase and the original size of the parent droplet [13]. In particular, the size of the dispersed phase impacts the occurrence frequency of the micro-explosive breakup [13].

Some experimental studies [14–17] aim at determining the integral ignition and combustion characteristics of droplets containing multiple fuel components. The main emphasis is on child-droplet sizes and velocities in a mist cloud. These characteristics depend much on the breakup regime (puffing or micro-explosion) [14,15]. Avulapati et al. [14] established that larger secondary fragments with radii of over 10 μm are much less likely to emerge from micro-explosion than from puffing. According to Rao et al. [15], an abrupt explosion produces smaller child droplets than a micro-explosion does. Puffing and micro-explosion occur due to the collapse of a bubble inside the droplet, whereas an abrupt explosion takes place without any noticeable bubble inside the droplet and leads to complete disintegration of parent droplet. The sizes of child droplets also depend on the component composition and structure of the parent droplet [15]. Ojha et al. [16] present child droplet velocity distributions against their diameters. The findings demonstrate [16] that the velocities of child droplets increase and their size decreases with an increase in the proportion of solid additives. Avulapati et al. [17] identified two types of micro-explosion accompanied by a stronger and weaker vapor expulsion with significantly different vapor concentrations and vaporization rates. The droplets in a strong vapor expulsion are larger and their velocities are higher than in the case of a weak vapor expulsion. Smaller child droplets and their higher velocities improve the homogenization of components of a gas-vapor mixture in combustion chambers of Diesel engines and systems of thermal and flame water treatment. They are likely to play an even more significant role when the distances between parent droplets are short, and synergistic or collective effects act on them.

Refs. [18,19] presented interaction regime maps for collisions of liquid droplets in a gas. The research findings given here build on these data. A number of aspects established in this research can be explained by analyzing the experimental findings on collisions between two-phase droplets in a gas [18]. In particular, in this paper significantly different collision outcomes were observed for secondary fragments of the first droplet interacting with the second and third one in the experiments with different distances between parent droplets. There are two main reasons for this. On the one hand, a rise of average and surface droplet temperature reduces the surface tension and viscosity of liquids, intensifies the droplet surface transformation in a flow, and contributes to bubble nucleation, which stimulates the destruction of near-surface layers and droplet breakup as a whole. On the other hand, the rapid liquid evaporation leads to the formation of buffer vapor layers around droplets serving as a thermal protection. The reference temperature (temperature of vapor and gas mixture) in these layers goes down relative to the gas temperature due to the fast endothermic phase transitions.

The significantly different fragmentations of the first, second, and third parent droplets are caused by different temperatures and velocity fields around them. For the same reasons, their heating and evaporation rates in the recording zone differ as well. Earlier research on the recording of thermal and aerodynamic traces [20] established that the droplet trace sizes can be controlled by altering the velocity and temperature of the oncoming flow. With this in mind, here we estimated the changes in the impact of these traces on breakup outcomes. With a decrease in the velocity of the oncoming flow and increase in its temperature, the trace became wider, and the following droplets did not deform much. However, if we increased the flow velocity and decreased its temperature, on the contrary, the trace behind each subsequent droplet became narrower, and the surfaces of all the droplets deformed significantly. In gas-vapor-droplet applications, droplets move quite chaotically in the flow, i.e., lead droplets shift continuously relative to the trajectories of subsequent droplets. In such conditions it is important to understand how to control the temperature distributions around droplets in different echelons. The first series of experiments [21] showed the droplet arrangement schemes to provide a reliable prediction of the liquid droplet temperature.

Using the experimental findings on the droplets going through deformation cycles [22], it is possible to predict the differences in the group effects of droplet fragmentation in the present research. In particular, the more non-spherical a droplet was, the larger its surface area was and hence the faster it heated up to reach the breakup conditions. If it stretched in the opposite direction of the flow, i.e., inflated like a parachute, local fragmentation was observed with the liquid chains breaking up into a polydisperse mist. If the droplet had a spherical or ellipsoidal shape stretched in the direction of the traveling flow, inertial heating took place, energy was accumulated near the gas/liquid interface, and a droplet broke up in the micro-explosion regime. At the same time, the analysis of the earlier researches of micro-explosion phenomena [23,24] indicates that the thinner the combustible shell was around the water core, the faster it heated up. The conditions for the vapor bubble nucleation at the water/Diesel fuel interface emerged in this very zone. Thus, we can conclude that the droplet shape has a significant impact on the droplet heating time until breakup, and the longer the heating, the more often micro-explosion occurred compared to puffing. The interaction with secondary fragments of neighboring droplets is not the only cause of changes to the parent droplet shapes. Also important is the droplet flow spinning, which is often employed in real applications, when droplet flows do not only go through deformation cycles due to thermogravitational convection but also spin rapidly. In such conditions, droplets heat faster, and liquid layers mix faster as well. Earlier research has shown [9] that the mixing of liquids slows down the superheating until breakup conditions and contributes to a shift from the prevalence of micro-explosion to puffing. Therefore, we can conclude that the droplet flow spinning is not feasible in the systems meant to intensify the secondary atomization of droplets in the micro-explosion regime. With such systems, it is much more effective to provide droplet hovering in a gas.

The aim of this research is to estimate the contribution of the joint impact of adjacent droplets in a group on the characteristics of child droplets emerging from the micro-explosive breakup as part of experiments with several typical liquid blends. The analysis of data from Refs. [9,21,25] indicates that experiments should be carried out with varying proportions liquids in a droplet (as emulsions or blends) to cover such applications as fuel combustion, thermal and flame water treatment, firefighting, etc. Antonov et al. [9] established that micro-explosion and puffing occur consistently with varying relative volume concentration of combustible and noncombustible liquids in a droplet in the range of 10%–90%. They also show [9] that more secondary fragments are provided by heating composite droplets compared to emulsion droplets. By composite droplets we mean unmixed two-liquid droplets prepared without adding stabilizers, emulsifiers, or surfactants. The water/fuel interface is clearly visible in these droplets. Emulsions, however, are prepared using additives: these are required to reduce the interfacial tension and to form the stable dispersed phase. In terms of estimating the collective effects on the success rate of micro-explosion, it is interesting to study these effects in a group of composite droplets with a volume concentration of combustible and noncombustible liquids from 10% to 90%. Ref. [21] presents the results of the first stage of research with a group of droplets establishing significant differences in the temperature of each of the droplets before fragmentation. Lead droplets are found to have a considerable impact on the temperature fields of their neighboring droplets. It is shown that the temperature regimes in a group of droplets can be adjusted by varying the distance between droplets. Here we present the findings of the second stage of research. We recorded the differences between the characteristics of secondary fragments from the breakup of three droplets in a group and identified the collective effects to establish the dependences of the number and size of secondary

fragments on the distances between parent droplets. This is the first research describing the collective influence of the distance between neighboring droplets in a group on the characteristics of child droplets produced by puffing/micro-explosion (child droplet radii and number). Earlier studies in this field [21,26] showed that the distance between neighboring droplets significantly influence on puffing/micro-explosion delay times in combination with effects of gas temperature, droplet radii and droplet compositions [27]. No results have been published so far analyzing the impact of the distance between neighboring droplets on child droplet characteristics (child droplet radii and number). Note that in this paper to be estimate only effects of distance between neighboring droplets. Gas temperature, droplet radii and droplet compositions assumed identical in the series of experiments.

2. Experimental techniques

2.1. Materials

The outcomes of micro-explosive fragmentation of three droplets with varying distance between them were studied using two liquids, typical of fuel and energy applications: Diesel fuel and water. Like at the first stage [21], these experiments involved liquids with the following volume concentrations: 90 vol% of Diesel fuel, 10 vol% of water and 10 vol% of Diesel fuel, 90 vol% of water. The choice of the liquids and their concentrations was based on the information from Ref. [9] that micro-explosion and puffing occurred consistently for these fuel blends in a wide range of temperatures (400–800 K) and original sizes of parent droplets (0.5–1 mm). Compositions with varying water concentration have different effective properties. In the present research, we focused on stable droplets: unmixed two-liquid droplets with a clearly discernible water/fuel interface. We chose two fuel compositions with different water concentrations (10 vol% and 90 vol%) because our research is aimed at developing a set of practical applications (fuel combustion, thermal and flame water treatment, firefighting). Some of them (fuel combustion) use a low proportion of water, while others (thermal and flame water treatment, firefighting) on the contrary use a low proportion of fuel. Table 1 shows the main properties of liquids (based on data from Ref. [28]) used in the experiments at their starting temperature of 300 K and temperature dependencies.

Droplets were generated in the same way as in Ref. [9]: using two electronic dispensers. At the first stage, a water droplet with a known volume was produced and suspended on a holder. After that, a Diesel fuel was formed which enveloped the water droplet, forming a film with a thickness of 0.05–0.5 mm [25]. The thickness of the Diesel fuel film depended on the volume of the droplet to be generated. Thus, a water core and a Diesel fuel shell were formed. As part of emulsified fuel combustion, water droplets are often dissolved in a combustible liquid and merge into one drop when heated [25], hence the choice of this water-Diesel droplet generation scheme. It is also typical of these applications to use two spray nozzles to inject the combustible and noncombustible liquids separately, so that they form two-liquid droplets right in the combustion chamber. These component injection techniques hold economic and technological promise.

2.2. Experimental setup

Fig. 1 shows the appearance and layout of the setup used in the experiments. It consists of the following main components: Phantom MIRO M310 high-speed CMOS video camera (monochrome; resolution up to 1280 × 800 pix; frame rate up to $6.5{\cdot}10^5$ fps); Nikon 200 mm f/4.0D IF-ED AF Micro-Nikkor lens (focal length: 200 mm, aperture range: *f*4–*f*32); Finnpipette Novus electronic dispensers (0.1 μl increment); nichrome wire holders, 0.2 mm in diameter; a Loip LF 50/500–1200 muffle furnace with a hollow ceramic tube (inner diameter 50 mm, length 500 mm); Multiled PT-V9 GS Vitec LED spotlight (continuous operating mode, 24 LEDs, 7700 Lumen total, 84 W, scattering angle 30°); SPSh20-23017/2000Z mini-robotic arm; National Instruments temperature recording system; workstation; metal cylinder; group of three droplets. A muffle furnace was used as a vertically arranged heating system. The temperature can be varied in the range of 293–1523 K. Note that all experimental results in this paper were conducted mainly at the same air temperature of 600 ± 15 K to be convenient with the aim of this paper (estimation of the distance effect between neighboring droplets). This temperature is average in the range of gas temperature (400–800 K) for successful droplet fragmentation in a wide range of fuel blends and original sizes of parent droplets [9]. But some features of air temperature

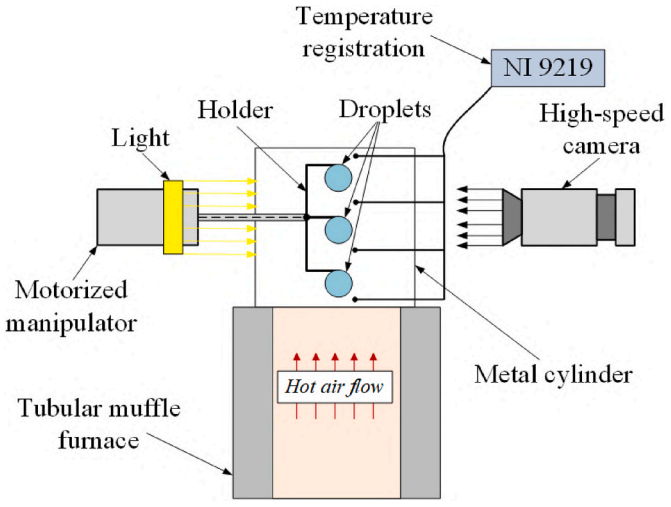

Fig. 1. Setup for recording the fragmentation behavior of three droplets in a group.

Table 1
Main properties of liquids (based on data from Ref. [28]) used in the experiments at their starting temperature of about 300 K and temperature dependencies.

	$T = 300$ K		Temperature dependencies (T in K)	
Liquid	Water	Diesel fuel	Water	Diesel fuel (n-dodecane)
Density, kg/m^3	998.2	878.7	$325{\cdot}0.27^{-\left[1-\left(\frac{T}{647.096}\right)\right]^{0.23}}$	$744.96 - 0.768067\cdot(T-300.0) + +0.000454\cdot(T-300.0)^2 - -0.00000328519\cdot(T-300.0)^3$
Heat capacity, J/(kg·K)	4182	1802	$\left(-2.2417{\cdot}10^4 + 876.97{\cdot}T - -2.5704{\cdot}T^2 + 2.4838{\cdot}10^{-3}{\cdot}T^3\right)\Big/18$	$2172.5 + 4.2017\cdot(T-300.0) - -0.0007\cdot(T-300.0)^2 + +0.000001673\cdot(T-300.0)^3$
Thermal conductivity, W/(m·K))	0.599	0.101	$-0.35667 + 5.057{\cdot}10^{-3}{\cdot}T - -6.1071{\cdot}10^{-6}{\cdot}T^2$	$0.2065 - 0.00022{\cdot}T$
Thermal diffusivity, mm^2/s	0.144	0.064	$0.034585 + 0.000362{\cdot}T$	$0.143351 - 0.000189{\cdot}T$
Dynamic viscosity, Pa·s	1.004	2.442	$3{\cdot}10^{-12}{\cdot}T^4 - 3.94{\cdot}10^{-9}{\cdot}T^3 + 2.0328{\cdot}10^{-6}{\cdot}T^2 - 4.6803{\cdot}10^{-4}{\cdot}T + +0.0406389$	$10^{-10.0687+1253/T+0.0137{\cdot}T-0.000012215{\cdot}T^2}$
Surface tension, N/m	0.072	0.029	$0.132674\cdot(1-T/647.13)^{0.955}$	$0.055717\cdot(1-T/658.2)^{1.3325}$

effects were presented in the paper in the wide range of temperature from 400 K to 800 K. A thermally insulated metal cylinder with three orifices was installed on top of the muffle furnace to provide the constant temperature at the outlet of the furnace. The orifices in the cylinder were used to introduce the droplets into the heating zone, record the breakup processes, and illuminate the droplets by a led spotlight. The droplets under study were placed into the recording area using a mini-robotic arm with three nichrome wires, arranged one above another on a holder. The distance between the first droplet and the heater exit was 5.0 ± 0.1 cm. Compared to other materials (phosphorus, ceramics, iron, steel, etc.) [29] and droplet fixation schemes on the holder, a nichrome wire showed the least interference with the heating, evaporation, and fragmentation of droplets under study. These evaluations were reported in Ref. [29] by comparing the experimental and theoretical research findings. The recording area was illuminated using a led spotlight for shadowgraphy. The droplet heating, evaporation, and breakup characteristics were recorded using a high-speed camera with a frame rate of 2000 fps at 512 × 768 pix resolution. The experimental video fragments were processed in the Phantom Camera Control software to analyze the initial droplet size before they enter the heating zone and to estimate the distance between them. The systematic errors in the measurement of these parameters did not exceed 0.025 mm and 0.05 mm, respectively. The systematic error in the distance measurements was defined by the magnitude of the scale factor and equaled 1–2 pix. Random errors Δ_r were estimated as $\Delta_r = t\,(\alpha_c,n)S_n$, where $t\,(\alpha_c, n)$ is the Student's coefficient, depending on the number of measurements n and confidence level α_c, taken equal to 0.95; S_n is the root squared deviation. Each experiment was repeated at least 10–15 times. Random errors of the measurements did not exceed 5%. The initial droplet diameter was measured in two sections, and then the average droplet diameter was defined as $D = (D_x + D_y)/2$ and the radius as $R_d = D/2$ where D_x and D_y are the x- and y-axis diameter respectively.

The local gas temperature in the cylinder was recorded by a system consisting of a National Instruments data collection module and a set of fast thermocouples (thickness is about 0.2 mm) with a measurement accuracy of at least ± 3 K and response time of less than 0.1 s. To calibrate the system, the temperature in the centre of cylinder was measured in several sections of the flow at different distances from the outlet with an increment of 1 cm at different temperatures in the muffle furnace. The temperature measurement scheme and the data obtained are given in Ref. [21]. To minimize the impact of temperature gradient on the droplet micro-explosion behavior, we chose the optimal distance from the outlet of the muffle furnace (3–4 cm) that provided a constant temperature in the recording area (variations of no more than 15 K [21]).

2.3. Number and size of secondary fragments

The number (N_{cd}) and radii (r_{cd}) of secondary fragments (child droplets) were analyzed by shadowgraphy (SP). We used three approaches to improve the accuracy of the experimental findings and estimate their repeatability in a series of experiments. The measurements, conducted using three different approaches, did not deviate by more than 5%. This result is crucial because it indicates that any of the three methods of recording the above characteristics is applicable in such series of experiments. The first method involved an in-house software code written in Mathematica and clarified in Ref. [25]. The moments of parent droplets breaking up into child droplets were identified on the images, converted to the tiff format, and imported into Mathematica. The application for the analysis of breakup outcomes of two-liquid droplets consisted of two parts: search of the binarization threshold (1) and the main process (2) involving the identification of the elements as well as the calculation of their number and size with respect to the scale factor. The binarization threshold was found automatically for the entire image using Otsu's method. Otsu's method chooses a threshold that minimizes the intraclass variance of the thresholded black and white pixels. The background subtraction was performed at each stage. The child droplets were marked with the help of the key functions of the main engine: Morphological Binarize and Median filter. Each marked object was represented by a spherical droplet of the same size as the marked object. After that we calculated the number of liquid fragments and the size of the highlighted child droplets. The size of the child droplets was measured with an accuracy of at least ±4%. The actual size (radius) of secondary droplets was derived from the area they occupied. We used formula $(S/4\pi)^{0.5}$ and the results of a series of 5–10 experiments under identical conditions (temperature, initial droplet size, liquid concentration, distance between adjacent droplets, etc.). The data in a series of measurements did not differ by more than 4%. In addition to our processing algorithm, we explored the breakup outcomes using the SP technique developed in the Actual Flow software package [30]. The experimental videos were broken down into frames and the frames were selected showing the emergence of child droplets. The images were further processed by several consecutive actions. At the first stage, we reduced the noise level using low-frequency filtration. Then we binarized the resulting images with the help of the Laplacian filter. At third processing stage, we searched for simply connected domains using the binarized image. Ultimately, an irregular data field was created for each image containing the droplet radii as well as the coordinates of droplet centers. At the last stage, the particles created by droplet flares were excluded from the images. The accuracy of child droplet size measurement by SP in Actual Flow was ±3%.

The number (N_{cd}) and size (r_{cd}) of child droplets were calculated from the images using a code developed in the Matlab software. In addition to the number and size of secondary fragments, this code determined the minimum, maximum, and average sizes, velocities, and kinetic energy of child droplets as well as the evaporation surface area after and before droplet breakup. Using the initial images obtained in the course of experiments, we determined the moments when parent droplets broke up into secondary fragments, i.e., child droplets. Two consecutive frames showing puffing/micro-explosion were saved, converted to tiff, and imported to the Matlab software. Processing involved the search of simply connected domains using the binarized image. The binarization procedure was the same as in Mathematica. As a result, an irregular data field was produced for each image containing the droplet radii and the coordinates of droplet centers. After that we selected a rectangular recording area of secondary droplets to search for them. The opportunity to choose a certain recording area of secondary fragments made it possible to determine the characteristics of secondary fragments for each of the droplets in a group. The maximum error in the calculation of child droplet sizes (radii) in Matlab software in the series of 5–10 experiments did not exceed 3% compared to the data obtained using other methods. Fig. 2 shows an example of image processing using the Matlab software. Note that during image processing we observed a considerable shift of secondary droplets at a frame rate of 2000 fps, stemming from the high velocity of secondary fragments. We increased the frame rate at the moment of fragmentation to 100,000 fps to eliminate smearing and improve the measurement accuracy. In this case, the inaccuracy of measuring the size of secondary droplets at their maximum velocity (~5 m/s) did not exceed 0.05 mm, which corresponded to the high frame rate (~100,000 frames per second) at the moment of breakup.

The image processing using the above approaches did not only involve image binarization but also the determination of the focal depth of the lens to count the number of droplets in the focal depth and beyond it. The secondary fragments outside the focal depth of the lens were factored in by conducting additional experiments with varying focal depth to calculate the adjustment coefficients. The number and sizes of secondary fragments were multiplied by these coefficients. The lens was focused manually for all the experiments using the Multi-Function Calibration Target (for Low Magnification Systems). With this target, we determined the focal depth of the lens. The target was placed in the recording area, and the focus was set manually to the zero mark. The

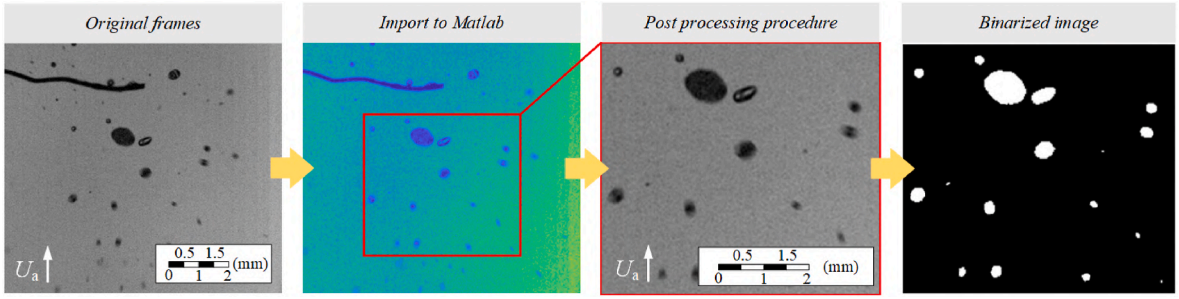

Fig. 2. Typical example of image processing using Matlab software for calculating the number and sizes of secondary fragments after the breakup of a parent droplet.

distance to the next visible mark on the target was the focal depth. The scale factor was determined in the same way. The grid was selected so that the typical droplet size was three times larger than the scale factor. The smallest droplets generated through the micro-explosive breakup of parent droplets occupied at least 3 pix. According to the scale factor used in this study, that was 0.075 mm. The size of the recording area was between 10 × 10 mm and 15 × 15 mm. In this research, the scale factor is the ratio of the numerical value of a certain physical magnitude to the length of the line segment in millimeters representing this magnitude. Here we measured the sizes and distances by image processing, so they were first obtained in pixels. The scale factor indicates how many millimeters are represented by one pixel in the image (unit of measurement: [mm/pix]). One can multiply the distance between two points obtained in pixels by the scale factor to obtain this distance in millimeters. The scale factor was defined using a calibration target [18]. The minimum registered diameter of child droplets in this research was 0.075 mm. Note that more detailed experimental technique based on modern high-speed cameras with higher resolution and frames rates can provide registration of very small child-droplets with diameters even less 0.075 mm [17]. But main tendency of child droplets characteristics described in this paper will not change significantly.

The atomization efficiency was determined by calculating the post-breakup free surface area of the liquid (S_1=N_{cd}·4·π·r_{cd}^2) and the pre-breakup free surface (S_0 = 4·π·R_{d0}^2). Not all the newly formed child droplets were in the recording area, so we calculated the droplet volumes after the collision (V_{cd} = 4/3·π·∑N_{cd}·r_{cd}^3) and before the collision (V_0 = 4/3·π·R_d^3). After that we increased the number of secondary fragments in proportion to their size to make the condition V_0=V_{cd} hold. The resulting ratio of the pre- and post-breakup liquid surface areas was given by

$$S_1 / S_0 = \left(N_{cd} \cdot 4\pi r_{cd}^2\right) / \left(4\pi R_d^2\right) = \frac{N_{cd} \cdot r_{cd}^2}{R_d^2} = \frac{V_0 r_{cd}^2}{V_{cd} R_d^2} = \frac{4/3\pi R_d^3 r_{cd}^2}{4/3\pi r_{cd}^3 R_d^2} = \frac{R_d}{r_{cd}}.$$

We used an in-house programming code written in the Matlab software because it exhibited good agreement with the results obtained using other approaches. Three approaches to post-processing were used to ensure that the results are independent of the approach selected.

3. Results and discussion

Fig. 3 shows typical images of two-liquid droplets breaking up in the puffing/micro-explosion regime with three distances between them (l = 3.5–9.8 mm). Note that the temperatures in the images refer to gas temperatures with droplets and time t = 3.2 s. The initial temperature distribution without droplets was 604 ± 10 K. The image processing established that lead droplets located upstream may affect the heating, evaporation, and micro-explosive breakup of neighboring droplets in different ways. Lead droplets typically break up in the puffing or micro-explosion regime depending on the heating conditions. Middle and downstream droplets do not only break up in the puffing and micro-explosion regime but may also evaporate steadily with a considerable decrease in temperature near their surface due to the impact of lead droplets. This is related to different water/fuel interface heating rate, i.e., the water/fuel interface of the lead droplet is almost always heated up faster than that of the middle and downstream droplets [21]. This happens because the heated gas flow oncoming on the lead droplet blows off the vapors formed on its surface and sweeps them to the area behind the droplet. This area is also referred to as a temperature trace. The images of these processes are given in Supplementary material A. The experimental findings have shown [20] that the typical sizes of a temperature trace behind a droplet are (5–7)R_d. By the temperature trace we mean the area of the ambient gas located behind the droplet, in which the temperature was lower due to evaporation. Thus, the occurrence of different breakup regimes can be ensured by altering the temperature and distance between droplets. The experiments have also established that the child droplets formed during micro-explosions can initiate the breakup of neighboring droplets by colliding with them. These effects become noticeable with a decrease in the inter-droplet distance. The closer the parent droplets are to each other, the more likely the collisions between parent droplets and child droplets will result in the micro-explosion of the latter. This effect was mostly observed for droplets in which intense vaporization took place, i.e., the droplet breakup was initiated by the destruction of its liquid envelope. The surface of parent droplets transformed significantly as a result of collisions; we also observed the intense mixing of liquids in the droplets. Even a grazing collision with small secondary fragments is enough to intensify these effects. Similar effects were observed in the experiments in Ref. [25] with a group of droplets free-falling in a high-temperature gaseous medium. The corresponding images are given in Supplementary material B.

The analysis of the images obtained in the experiments identified some consistent patterns in the interaction between secondary fragments of the first droplet (leading the oncoming flow) with the following two droplets (Supplementary material C). In particular, we found the conditions in which child droplets interacted with liquid layers and bubbles of the second and third droplet. Droplet collisions occurred in one of the four known interaction regimes: coalescence (merging), separation (collision accompanied by the deformation of liquid layers in both droplets, which then retain their original sizes and trajectories), bounce (elastic collision without mixing), and disruption (rapid atomization of parent droplets into a cloud of small secondary fragments). The occurrence of this or that regime depended on the resultant velocities of secondary droplets formed after the breakup of the first one as well as the impact angle (Supplementary material D). When the first parent droplet broke up into secondary droplets, their velocities mostly fell within the range of 1–15 m/s and depended on their sizes as well as the velocity and temperature of the oncoming air flow. The impact angles varied from 15° to 90°. Coalescence and bounce prevailed at low velocities and compact angles. Off-center collisions at low velocities were accompanied by bounce, i.e., elastic interaction without mixing of droplets. Images showed that phase transitions on the droplet surface played an important part in these conditions. In particular, rapid evaporation caused vapor outflow from the droplet surface in the direction opposite to the resultant vector of secondary fragments towards

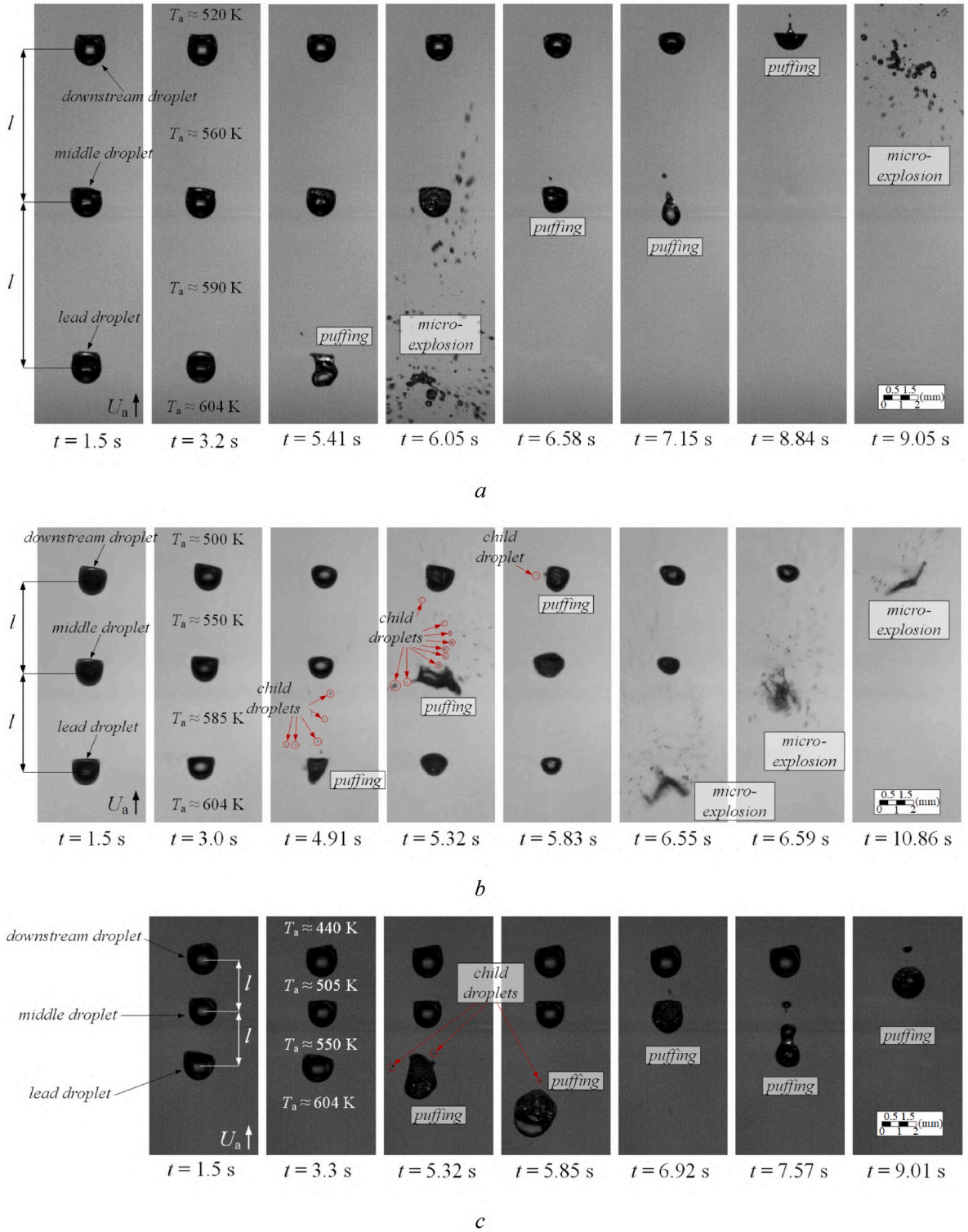

Fig. 3. Typical images showing the fragmentation of two-liquid droplets in a group of three droplets: *a* – Diesel fuel 90 vol%, water 10 vol%, T_{gas} without droplets was equal 604 ± 10 K, $l \approx 9.86$ mm, $R_{d0} \approx 0.88$ mm, *b* – Diesel fuel 90 vol%, water 10 vol%, T_{gas} without droplets was equal 604 ± 10 K, $l \approx 6.14$ mm, $R_{d0} \approx 0.84$ mm, *c* – Diesel fuel 10 vol%, water 90 vol%, T_{gas} without droplets was equal 604 ± 10 K, $l \approx 3.55$ mm, $R_{d0} \approx 0.81$ mm).

the second and third parent droplets (Supplementary material E). This slowed down the droplets before collision. As a result, repulsive forces and surface tension contributed to droplet bounce. Head-on collisions mostly resulted in droplet coalescence. Separation and disruption were observed at higher resultant velocities of secondary fragments from the first droplet towards the second and third one. The analysis of images (Fig. 3) established that the structure of the second and third droplets before collision played an important part. If they had vaporization centers (bubbles), hits of secondary fragments of the first droplet led to the destruction of these bubbles, and secondary fragments broke off from the surface of the second and third droplets. However, if the second and third droplets were homogeneous enough (without vapor bubbles inside), the secondary fragments of the first droplet moving at high speed pierced through the liquid layers and left the second and third

droplets behind, i.e., the separation outcome prevailed. The balance of inertia and surface tension forces in the collision zone was important as well.

Overall, the analysis of images (Fig. 3) has shown that an array of secondary fragments from the first disintegrated droplet moves in a gas flow (in the direction of its upward movement) in the form of fragmentation projectiles. In other words, the child droplets moved in a more or less straight line with the exception of the few large secondary fragments, 2–3 times larger than average. These deviated from the linear trajectories under the opposing forces of inertia and gravity, spun in the flow and even hovered for some time; however, they lost a certain volume of liquid due to fast evaporation and were entrained upwards with the flow. These fragments broke up in a chain-like way in the recording area. As a rule, the consecutive fragmentation of child droplets occurred in the micro-explosion regime because their temperature was high enough and their surface layers transformed considerably after they emerged. In these droplets we observed the vaporization centers in the form of water/liquid combustible component interface, almost without bubbles (they had left the droplet during the primary breakup). These conditions contributed to the local superheating of the inter-component interface until the breakup in the micro-explosion regime. The effects of consecutive breakups were recorded in the experiments. Child droplets broke up in the micro-explosion regime.

Fig. 3 as well as Supplementary materials A and B show that parent droplets are not at rest on holders when heated. This factor is crucial because it demonstrates that the surface of heterogeneous droplets can be significantly transformed not only during their free fall or injection into operating chambers but also when sitting on the walls. Intense transformation of both near-surface and deep liquid layers of droplets was recorded even after a short-term droplet contact with rods, for instance, when a droplet broke off from one holder and then interacted with the second holder. The conditions of bubble nucleation in such droplets were as follows: a local superheated zone was formed with temperatures close to the liquid boiling point at the moment of droplet contact with the holder. It was also established that when heated droplets broke off from one holder and got to the second one, they did not spread over it as intensely as over the first one. At first sight, this result does not seem obvious due to a considerable decrease in the surface tension of the liquid layers. It can be attributed to the fact that a droplet was placed on the first holder under normal conditions and then introduced into the heating zone by a motorized manipulator. When heated, its contact area with a holder decreased due to liquid evaporation, droplet shrinking, as well as the ascending air flow pressing it against the holder surface. A droplet only broke off from the holder after puffing. This collision outcome means the heating of a certain volume of liquid until near-boiling conditions. Under such conditions, vapors are rapidly blown away from the droplet surface. Due to their outflow, a buffer vapor zone is formed around the droplet. Superheating leads to fragmentation. Near-surface layers are unstable. This intensifies the break-off of the droplet from the holder. As it approaches a dry surface of the holder that is placed lower, it only sticks to the holder by a small portion of its surface. Then its heating causes it to shift along the holder and transform; however, it does not spread as much as at the start when it was introduced into the heating zone. The images (Fig. 3) of the experiments show that the droplets exposed to a rapidly oncoming air flow deformed into oblate ellipsoids and half-spheres in all cases. Free-falling droplets in a gas take the so-called tear-drop shape and go through a certain deformation cycle, changing their shapes from an oblong ellipsoid to a sphere and to an oblate ellipsoid. The temperature and aerodynamic traces are of different sizes for each of these shapes due to significant differences in the aerodynamic forces acting on them. Note that it is exactly true that the alignment of droplets in the streamwise direction is very important. But in real experiments there is some deviation of this postulate. It is very difficult to control strong alignment of droplets in the streamwise direction. The deviation of droplets along the main streamwise direction in current research was always less than $R_{d0}/2$. The such deviation ($R_{d0}/2$) was led errors of child droplets sizes measurements but no more than 3%.

Figs. 4 and 5 present the size distributions of secondary fragments with varying distance between parent droplets from 9.86 mm to 3.55 mm for the two blends: Diesel fuel 10 vol%, water 90 vol% and Diesel fuel 90 vol%, water 10 vol% at $T_a = 604$ K. As can be seen from Figs. 4 and 5, the greatest number of child droplets with minimum sizes as well as maximum surface area ratios is observed for the lead droplet in all experimental conditions. Also, when the distance between droplets is the longest, the difference in the post-breakup to pre-breakup area ratio is minimal for the lead, middle, and downstream droplets, i.e., the mutual influence of droplets is at the minimum. This effect was especially pronounced with the shortest distance between neighboring droplets. Note that effect of time-dependent variation of the droplet sizes before puffing/micro-explosion was presented in our earlier research [31] (see Fig. 6).

The size distributions of secondary droplets indicate that the greater the distance between parent droplets, the more secondary fragments are formed from the breakup of each of them and the smaller the average size of the child droplets. This trend was true for all the experiments carried out with different arrangements of water and combustible liquid in the parent droplets. This can be attributed to two main reasons. First, the greater the distance between parent droplets located in series in a flow, the higher the temperature of the gas-vapor mixture around each of them. The impact of adjacent droplets on the temperature field of the overall system was weakly pronounced, so their heating and evaporation rates were high. In such conditions, the emerging secondary fragments were small and shrank in size when heated in the flow. Second, small vapor-liquid fragments broke off from the surface of each droplet being heated and interacted with neighboring droplets. These small fragments were vapor bubbles with a thin liquid shell. When they contacted adjacent parent droplets, additional vaporization centers were formed in the latter, which intensified their subsequent fragmentation.

Figs. 4 and 5 show that the liquid surface area ratio can be varied in the range of 7–14 by altering the distance between parent droplets at a gas flow temperature of about 604 K. The maximum values of S_1/S_0 can exceed 100. Therefore, the required values of S_1/S_0 can be provided by a composite system varying the gas temperature and the distance between parent droplets characterizing the droplet size distribution in a mist. The component concentration ratio in parent droplets is a limiting factor. In particular, when comparing Figs. 4 and 5, it is necessary to underline the much smaller values of S_1/S_0 and the number of secondary fragments in the experiments with droplets containing more water than combustible liquid. There are several reasons for that. First, water has a much higher heat capacity and vaporization heat than combustible liquids do. Therefore, a droplet with a higher water concentration is heated to lower temperatures within the same period of time compared to a droplet containing more combustible liquid. Second, the vast majority of emerging secondary droplets are fragments with the prevailing water content. Thus, they do not evaporate as fast as the fragments containing the combustible liquid. Third, the proportion of medium-sized secondary fragments is much higher in the experiments with the parent droplets in which the water content dominated. This is attributed to the shift in the transition from the micro-explosion regime to puffing with an increase in the water concentration in two-liquid parent droplets. The minimum radii of secondary fragments in Figs. 4 and 5 were identical (0.05 mm). This is caused by the resolution of the video recording system (camera, lens, and spotlights). In particular, with the settings used in the experiments, the fragments smaller than 0.05 mm were still detected, but they occupied a limited number of pixels on the video frame, which was the identification limit, i.e., within the measurement error. With a recording system with a greater focal depth and resolution, it is possible to establish more precise limits as to the minimum size of secondary fragments. But their velocity as well as heating and evaporation rate will play an important part. In particular, we observed the conditions in which secondary fragments moved fast after their

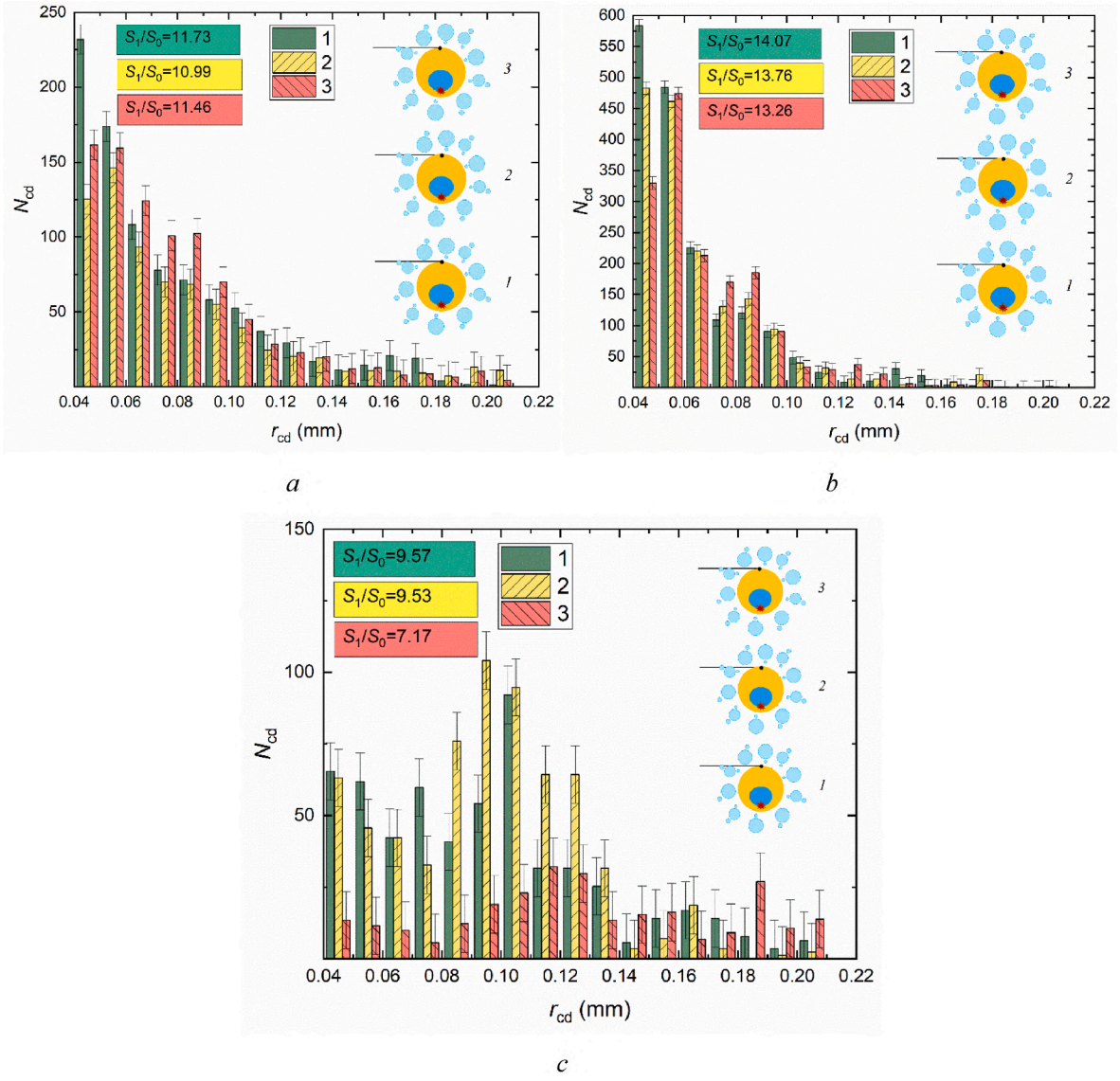

Fig. 4. Size distributions of secondary fragments with varying distance between droplets in a group: *1* – lead droplet, *2* – middle droplet, *3* – downstream droplet. Experimental parameters: Diesel fuel 10 vol%, water 90 vol%, $T_a = 604 \pm 10$ K, $R_{d0} = 0.91 \pm 0.02$ mm, $L = 9.86 \pm 0.05$ mm (*a*), $L = 6.48 \pm 0.04$ mm (*b*), $L = 3.55 \pm 0.05$ mm (*c*).

formation due to the shock wave and shrunk in size due to evaporation, when the whole droplet was still intact. In such conditions, it is important to employ an automatic tracking algorithm to track all the fragments formed as a result of the droplet breakup and sum them up to check if the volume of the parent droplet is equal to the volume of the array of child droplets. We used this algorithm in this study. Due to this algorithm, we managed to track an array of secondary fragments of different sizes traveling at different velocities in the recording area. The tracking algorithm allowed us infer that almost all the secondary fragments were spherical in shape despite their high velocities after a mist cloud was formed. Just a small fraction of large secondary fragments were ellipsoidal. Their average size was determined by measuring several maximum and minimum diameters in different sections. The higher the viscosity of the liquid was in a parent droplet, the fewer non-spherical droplets were formed. The corresponding conclusion was made after comparing the experimental data on the droplets with the dominating combustible liquid compared to water. The approximations for the evaporation surface area ratio after and before breakup as a function of the ratio of the inter-droplet distance to their original size (radius) are given in Table 2. These expressions can be used to predict the characteristics of secondary droplets as part of mathematical modeling.

Fig. 6 presents the size distributions of secondary fragments with varying air temperature from 400 K to 800 K for the blend: Diesel fuel 90 vol%, water 10 vol% at $L = 6.48 \pm 0.04$ mm and $R_{d0} = 0.9 \pm 0.02$ mm. As can be seen from Fig. 6, the greatest number of child droplets with minimum sizes as well as maximum surface area ratios is observed for the lead droplet in all experimental conditions. Also, when air temperature increased number of child droplets from lead, middle and downstream droplets increased as well as maximum surface area ratios. This is because the heat flux directed towards the droplet surface was much greater when the air temperature higher. This intensifies the heat transfer processes, thermocapillary and thermogravitational convection in the droplets. As a result, the conditions of micro-explosion breakup at the inter-component boundary are achieved rather quickly. The experimental conditions whereby tandem droplets in a heated medium are in good agreement with real-life liquid atomization technologies (high-potential gas-vapor-droplet technologies to intensify the evaporation of additives and the ignition of fuel compositions).

The energy balance of secondary fragments formed during micro-

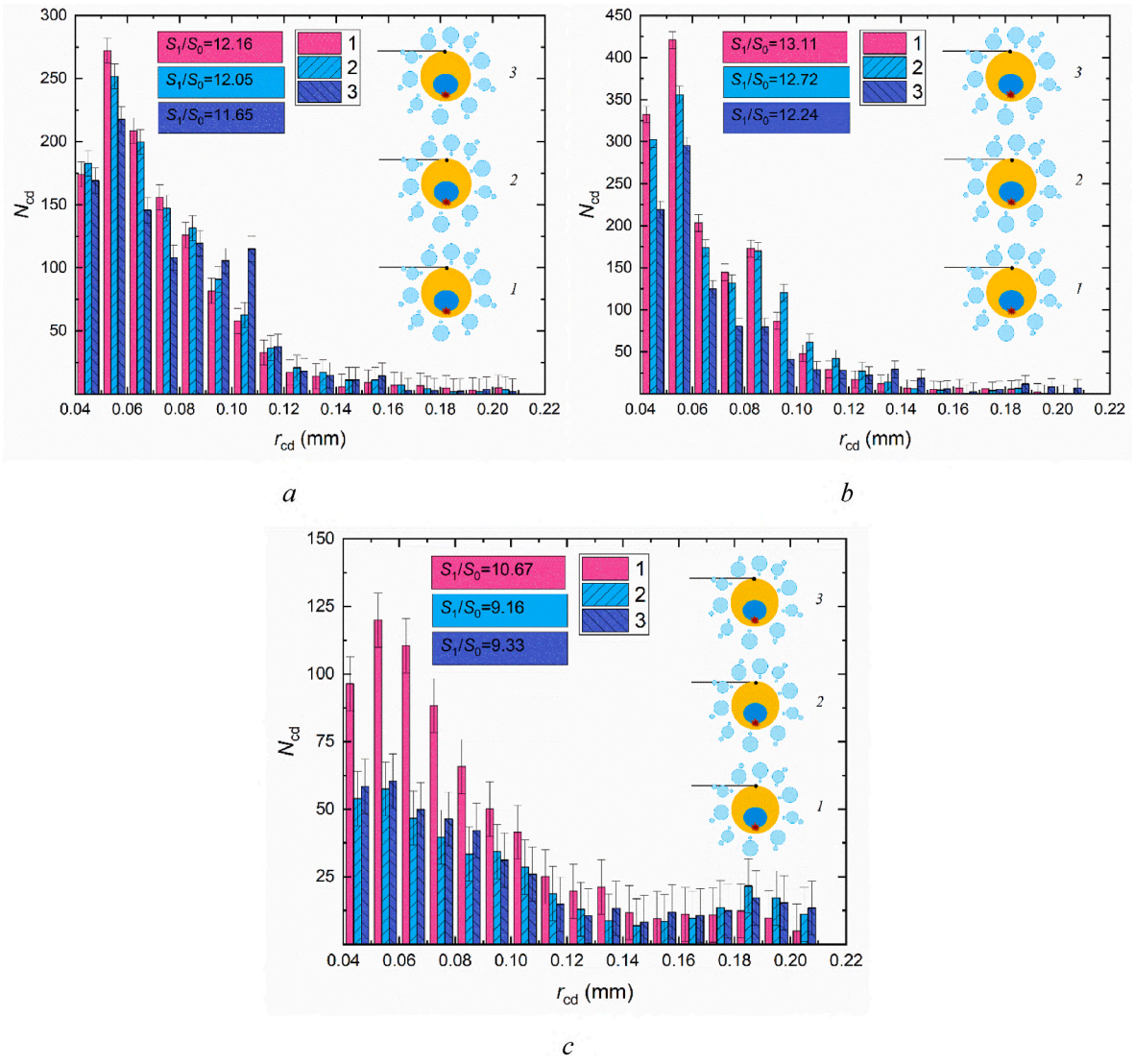

Fig. 5. Size distributions of secondary fragments with varying distance between droplets in a group: *1* – lead droplet, *2* – middle droplet, *3* – downstream droplet. Experimental parameters: Diesel fuel 90 vol%, water 10 vol%, $T_a = 604 \pm 10$ K, $R_{d0} = 0.9 \pm 0.02$ mm, $L = 9.86 \pm 0.06$ mm (*a*), $L = 6.48 \pm 0.04$ mm (*b*), $L = 3.55 \pm 0.04$ mm (*c*).

explosion is defined by their kinetic and surface energy. The results are presented as a ratio of the secondary fragments' surface energy to kinetic energy, similar to the inverse Weber number [7]:

$$\frac{\sigma 4\pi r_{cd}^2}{\frac{1}{2}m_{cd}\cdot u_{cd}^2} = \frac{12}{We} = f\left(\frac{1}{r_{cd}\cdot u_{cd}^2}\right).$$

Fig. 7 presents the experimentally established variation ranges of the ratio of the child droplets' surface energy to kinetic energy for two fuel blends: Diesel fuel 10 vol%, water 90 vol% (*a*) and Diesel fuel 90 vol%, water 10 vol% (*b*). The analysis of Fig. 7 shows that the variation ranges of the ratios of the surface to kinetic energies are virtually identical for different blends. Interesting aspects were established for droplets with different proportions of water and Diesel fuel. When the combustible liquid prevailed in the composition of the parent droplet, there were more secondary fragments than in the experiments with parent droplets with a high proportion of water. However, due to high heating and evaporation rates, small child droplets with Diesel fuel slowed down considerably in a gas, i.e., they traveled along the same path as the carrier gas but in the opposite direction. This effect leveled out the kinetic energy of secondary fragments as a whole. With the domination of water in the composition of the parent droplet, fewer secondary fragments were formed, but they had different trajectories, and due to their large size, not all of them followed the gas flow. Thus, the ratio of energies in a mist cloud of secondary fragments can be controlled by varying the proportion of water and combustible liquid in parent droplets. These ratios depend on the component composition of secondary fragments: they broke up repeatedly (and even in a chain-like way) when their structure was highly inhomogeneous. This contributed to the increase in the kinetic energy compared to potential energy. Here we should outline the earlier research findings [32] that demonstrated a significant impact of three rheological characteristics of liquids in droplets—surface tension, interfacial tension, and viscosity—on the collision outcomes for a group of three droplets. According to the research findings [32], the liquid viscosity and surface tension have a major impact on the number of secondary droplets and the energy ratio under study; the higher the surface tension and viscosity, the higher the surface to kinetic energy ratio. The energy ratio of secondary fragments with different proportions of water and combustible liquid can be varied in a wide range by using surfactants, stabilizers, solvents, and plasticizers. This conclusion shows great prospects for the micro-explosive droplet breakup as a method of secondary droplet atomization in applications with a high proportion of water in a liquid flow (for instance,

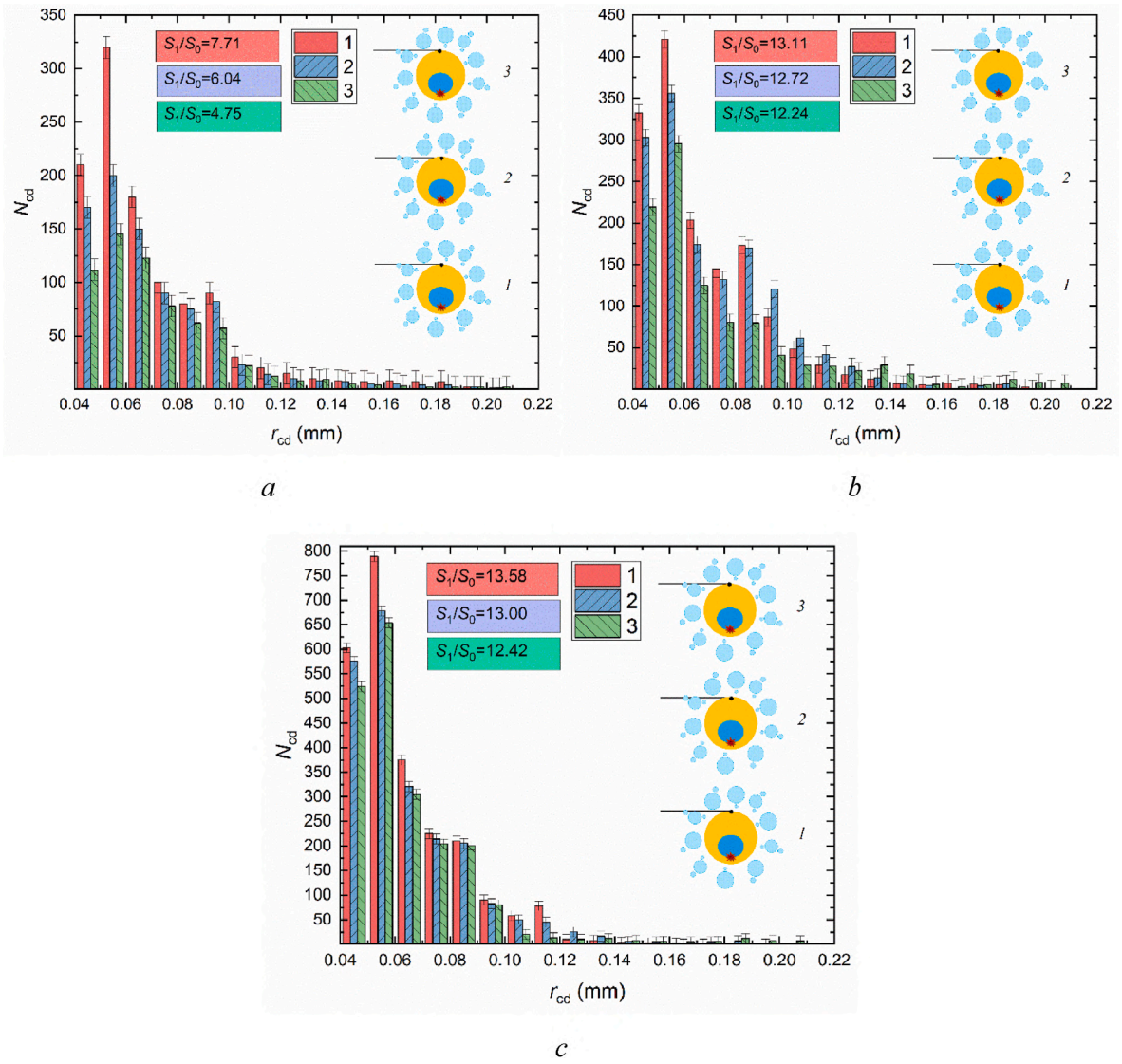

Fig. 6. Size distributions of secondary fragments with varying air temperature: *1* – lead droplet, *2* – middle droplet, *3* – downstream droplet. Experimental parameters: Diesel fuel 90 vol%, water 10 vol%, $L = 6.48 \pm 0.04$ mm, $R_{d0} = 0.9 \pm 0.02$ mm, $T_a = 400 \pm 10$ K (*a*), $T_a = 600 \pm 10$ K (*b*), $T_a = 800 \pm 10$ K (*c*).

Table 2
Approximations for the evaporation surface area ratio after and before breakup (S_1/S_0) as a function of the ratio of inter-droplet distance to their original size (radius) (L/R_{d0}).

Composition	Diesel fuel 10 vol%, water 90 vol%	Diesel fuel 90 vol%, water 10 vol%
Lead droplet	$S_1/S_0 = 7.522 \cdot (L/R_{d0})^{0.2298}$	$S_1/S_0 = 11.159 \cdot (L/R_{d0})^{0.067}$
Middle droplet	$S_1/S_0 = 8.1411 \cdot (L/R_{d0})^{0.1721}$	$S_1/S_0 = 11.009 \cdot (L/R_{d0})^{0.0429}$
Downstream droplet	$S_1/S_0 = 3.9898 \cdot (L/R_{d0})^{0.498}$	$S_1/S_0 = 7.7054 \cdot (L/R_{d0})^{0.1202}$

thermal and flame water treatment, heat and mass transfer systems, firefighting, and spray cooling). The ratio in Fig. 7 shows how much the kinetic energy of the moving secondary droplets in a group exceeds the surface energy of parent droplets. Thus, one can predict how much the heat power will increase due to micro-explosions. A detailed energy analysis of the effects of micro-explosions is presented in Ref. [33].

In line with the aim of this research, we studied the joint impact of the main factors—oncoming gas flow, distance between droplets, and the proportion of combustible and noncombustible component in their composition—on the characteristics of secondary fragments. The analysis of our earlier studies [9,21,25] indicates a large number of factors having a significant impact on the component composition, sizes, velocities, trajectories, momentum, and energy ratio of the secondary fragments, in particular: holder material and size, heating temperature and scheme, original droplet size, component composition and droplet generation scheme, concentration and size of solid particles. In the future, it is sensible to evaluate how these factors affect the joint chain-like atomization of a group of parent droplets in different arrangements in a gas. This will make it possible to produce an experimental database to develop physical and mathematical models simulating the micro-explosive fragmentation accounting for the synergistic effects of droplets breakup. These models would scale to chambers, reactors, and furnaces of various units and provide answers to important questions: which relative concentrations of the dispersed phase are necessary to intensify the secondary droplet atomization of sprayed liquids.

4. Conclusion

The experimental research established the size differences of secondary fragments formed during the breakup of several two-liquid droplets located at a variable distance from each other. These

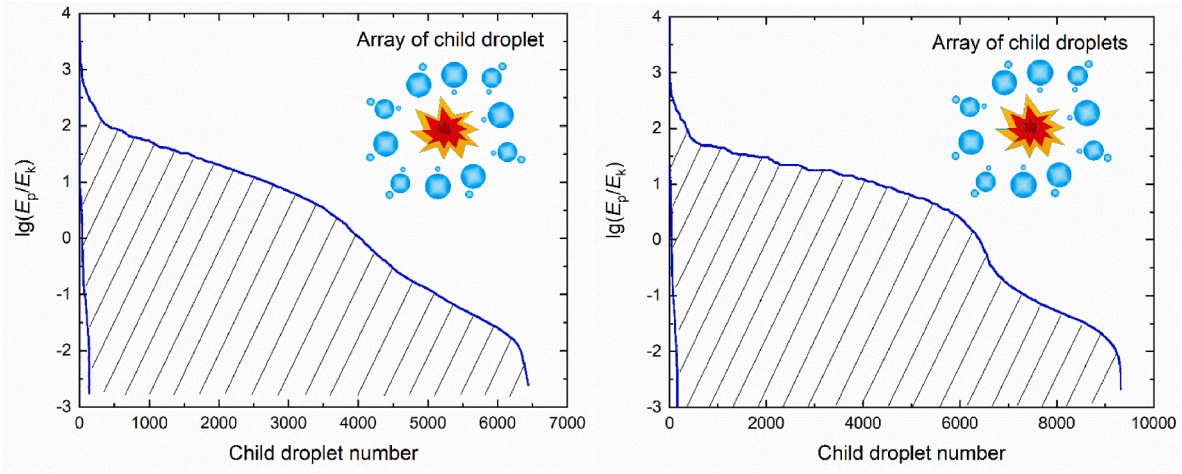

a *b*

Fig. 7. Range of energy ratio of the child droplets' surface energy to kinetic energy ratio in the series of experiments; $T_a = 604 \pm 10$ K, $R_{d0} = 0.91 \pm 0.02$ mm, $L = 9.86–3.55$ mm: Diesel fuel 10 vol%, water 90 vol% (*a*), Diesel fuel 90 vol%, water 10 vol% (*b*).

differences reflect the collective effects of explosive fragmentation occurring upon heating of an array of two-liquid droplets. Lead droplets moving along the trajectory of the heated air flow break up into a finer mist. The sizes of secondary fragments of each parent droplet can be controlled by varying the distance between subsequent parent droplets. In particular, if parent droplets are located at a distance of more than 8–10 radii from each other, the secondary fragments of each of them are practically the same in size, i.e., this arrangement density of the parent droplets will provide fuel fragments of similar size filling the chamber. When parent droplets are more densely arranged, their interactions with secondary droplets are observed. As a result of collisions between secondary fragments and parent droplets, one of the two fragmentation regimes occurs: puffing or micro-explosion.

Declaration of competing interest

The authors declare that they have no known competing financial interests or personal relationships that could have appeared to influence the work reported in this paper.

Data availability

No data was used for the research described in the article.

Acknowledgments

The research was funded by Russian Science Foundation (project No 21-71-10008, https://rscf.ru/project/21-71-10008/) (Dmitrii Antonov and Roman Fedorenko express their gratitude to the foundation for supporting research). Pavel Strizhak expresses his gratitude to the grant fund of the President of the Russian Federation (project MD-1616.2022.4) for supporting the development of a technique for tracking the interfluid boundary.

Appendix A. Supplementary data

Supplementary data to this article can be found online at https://doi.org/10.1016/j.ijthermalsci.2022.107858.

References

[1] S.S. Sazhin, Modelling of fuel droplet heating and evaporation: recent results and unsolved problems, Fuel 196 (2017) 69–101, https://doi.org/10.1016/j.fuel.2017.01.048.

[2] V. Ayhan, S. Tunca, Experimental investigation on using emulsified fuels with different biofuel additives in a DI diesel engine for performance and emissions, Appl. Therm. Eng. 129 (2018) 841–854, https://doi.org/10.1016/j.applthermaleng.2017.10.106.

[3] A. Alkhedhair, I. Jahn, H. Gurgenci, Z. Guan, S. He, Parametric study on spray cooling system for optimising nozzle design with pre-cooling application in natural draft dry cooling towers, Int. J. Therm. Sci. 104 (2016) 448–460, https://doi.org/10.1016/j.ijthermalsci.2016.02.004.

[4] S. Tonini, M. Gavaises, A. Theodorakakos, The role of droplet fragmentation in high-pressure evaporating diesel sprays, Int. J. Therm. Sci. 48 (2009) 554–572, https://doi.org/10.1016/j.ijthermalsci.2008.03.020.

[5] H. Fujimoto, A.Y. Tong, H. Takuda, Interaction phenomena of two water droplets successively impacting onto a solid surface, Int. J. Therm. Sci. 47 (2008) 229–236, https://doi.org/10.1016/j.ijthermalsci.2007.02.006.

[6] D. Tarlet, E. Mura, C. Josset, J. Bellettre, C. Allouis, P. Massoli, Distribution of thermal energy of child-droplets issued from an optimal micro-explosion, Int. J. Heat Mass Tran. 77 (2014) 1043–1054, https://doi.org/10.1016/j.ijheatmasstransfer.2014.06.054.

[7] D. Tarlet, C. Allouis, J. Bellettre, The balance between surface and kinetic energies within an optimal micro-explosion, Int. J. Therm. Sci. 107 (2016) 179–183, https://doi.org/10.1016/j.ijthermalsci.2016.04.008.

[8] D. Tarlet, J. Bellettre, M. Tazerout, C. Rahmouni, Prediction of micro-explosion delay of emulsified fuel droplets, Int. J. Therm. Sci. 48 (2009) 449–460, https://doi.org/10.1016/j.ijthermalsci.2008.05.005.

[9] D.V. Antonov, M.V. Piskunov, P.A. Strizhak, Breakup and explosion of droplets of two immiscible fluids and emulsions, Int. J. Therm. Sci. 142 (2019) 30–41, https://doi.org/10.1016/j.ijthermalsci.2019.04.011.

[10] A.M. Ithnin, H. Noge, H.A. Kadir, W. Jazair, An overview of utilizing water-in-diesel emulsion fuel in diesel engine and its potential research study, J. Energy Inst. 87 (2014) 273–288, https://doi.org/10.1016/j.joei.2014.04.002.

[11] S. Yoon, S. Lee, H. Kwon, J. Lee, S. Park, Effects of the swirl ratio and injector hole number on the combustion and emission characteristics of a light duty diesel engine, Appl. Therm. Eng. 142 (2018) 68–78, https://doi.org/10.1016/J.APPLTHERMALENG.2018.06.076.

[12] E. Mura, C. Josset, K. Loubar, G. Huchet, J. Bellettre, Effect of dispersed water droplet size in microexplosion phenomenon for water in oil emulsion, At. Sprays. 20 (9) (2010) 791–799, https://doi.org/10.1615/AtomizSpr.v20.i9.40.

[13] M. Yahaya Khan, Z.A. Abdul Karim, A.R.A. Aziz, M.R. Heikal, C. Crua, Puffing and microexplosion behavior of water in pure diesel emulsion droplets during leidenfrost effect, Combust. Sci. Technol. 189 (2017) 1186–1197, https://doi.org/10.1080/00102202.2016.1275593.

[14] M.M. Avulapati, L.C. Ganippa, J. Xia, A. Megaritis, Puffing and micro-explosion of diesel–biodiesel–ethanol blends, Fuel 166 (2016) 59–66, https://doi.org/10.1016/j.fuel.2015.10.107.

[15] D.C.K. Rao, S. Syam, S. Karmakar, R. Joarder, Experimental investigations on nucleation, bubble growth, and micro-explosion characteristics during the combustion of ethanol/Jet A-1 fuel droplets, Exp. Therm. Fluid Sci. 89 (2017) 284–294, https://doi.org/10.1016/j.expthermflusci.2017.08.025.

[16] P.K. Ojha, R. Maji, S. Karmakar, Effect of crystallinity on droplet regression and disruptive burning characteristics of nanofuel droplets containing amorphous and crystalline boron nanoparticles, Combust. Flame 188 (2018) 412–427, https://doi.org/10.1016/j.combustflame.2017.10.005.

[17] M.M. Avulapati, T. Megaritis, J. Xia, L. Ganippa, Experimental understanding on the dynamics of micro-explosion and puffing in ternary emulsion droplets, Fuel 239 (2019) 1284–1292, https://doi.org/10.1016/j.fuel.2018.11.112.

[18] P. Tkachenko, N. Shlegel, P. Strizhak, Collisions of two-phase liquid droplets in a heated gas medium, Entropy 23 (2021), https://doi.org/10.3390/e23111476.

[19] X. Jia, J.-C. Yang, J. Zhang, M.-J. Ni, An experimental investigation on the collision outcomes of binary liquid metal droplets, Int. J. Multiphas. Flow 116 (2019) 80–90, https://doi.org/10.1016/j.ijmultiphaseflow.2019.04.008.
[20] I. Voytkov, R. Volkov, P. Strizhak, Reducing the flue gases temperature by individual droplets, aerosol, and large water batches, Exp. Therm. Fluid Sci. 88 (2017) 301–316, https://doi.org/10.1016/j.expthermflusci.2017.06.009.
[21] D.V. Antonov, R.S. Volkov, R.M. Fedorenko, P.A. Strizhak, G. Castanet, S.S. Sazhin, Temperature measurements in a string of three closely spaced droplets before the start of puffing/micro-explosion: experimental results and modelling, Int. J. Heat Mass Tran. 181 (2021), 121837.
[22] R.S. Volkov, G.V. Kuznetsov, P.A. Strizhak, Water droplet deformation in gas stream: impact of temperature difference between liquid and gas, Int. J. Heat Mass Tran. 85 (2015) 1–11, https://doi.org/10.1016/j.ijheatmasstransfer.2015.01.078.
[23] D.V. Antonov, G.V. Kuznetsov, P.A. Strizhak, O. Rybdylova, S.S. Sazhin, Micro-explosion and autoignition of composite fuel/water droplets, Combust. Flame 210 (2019) 479–489, https://doi.org/10.1016/j.combustflame.2019.09.004.
[24] H. Watanabe, K. Okazaki, Visualization of secondary atomization in emulsified-fuel spray flow by shadow imaging, Proc. Combust. Inst. 34 (2013) 1651–1658, https://doi.org/10.1016/j.proci.2012.07.005.
[25] D.V. Antonov, G.V. Kuznetsov, P.A. Strizhak, Comparison of the characteristics of micro-explosion and ignition of two-fluid water-based droplets, emulsions and suspensions, moving in the high-temperature oxidizer medium, Acta Astronaut. 160 (2019) 258–269, https://doi.org/10.1016/j.actaastro.2019.04.048.
[26] D.V. Antonov, R.M. Fedorenko, P.A. Strizhak, G. Castanet, S.S. Sazhin, Puffing/micro-explosion of two closely spaced composite droplets in tandem: experimental results and modelling, Int. J. Heat Mass Tran. 176 (2021), https://doi.org/10.1016/j.ijheatmasstransfer.2021.121449.
[27] D.V. Antonov, R.M. Fedorenko, P.A. Strizhak, Child droplets produced by micro-explosion and puffing of two-component droplets, Appl. Therm. Eng. 164 (114501) (2019), https://doi.org/10.1016/j.applthermaleng.2019.114501.
[28] C. Yaws, L, Yaws' Handbook of Thermodynamic and Physical Properties of Chemical Compounds, Knovel, 2003.
[29] D. Antonov, J. Bellettre, D. Tarlet, P. Massoli, O. Vysokomornaya, M. Piskunov, Impact of holder materials on the heating and explosive breakup of two-component droplets, Energies 11 (3307) (2018), https://doi.org/10.3390/en11123307.
[30] Y.K. Akhmetbekov, S.V. Alekseenko, V.M. Dulin, D.M. Markovich, K.S. Pervunin, Planar fluorescence for round bubble imaging and its application for the study of an axisymmetric two-phase jet, in: Exp. Fluids, 2010, https://doi.org/10.1007/s00348-009-0797-0.
[31] R.M. Fedorenko, D.V. Antonov, P.A. Strizhak, S.S. Sazhin, Time evolution of composite fuel/water droplet radii before the start of puffing/micro-explosion, Int. J. Heat Mass Tran. 191 (2022), https://doi.org/10.1016/j.ijheatmasstransfer.2022.122838.
[32] D. V Antonov, G. V Kuznetsov, P.A. Strizhak, R.M. Fedorenko, Micro-explosion of droplets containing liquids with different viscosity, interfacial and surface tension, Chem. Eng. Res. Des. 158 (2020) 129–147, https://doi.org/10.1016/j.cherd.2020.03.029.
[33] D.V. Antonov, N.E. Shlegel, P.A. Strizhak, D. Tarlet, J. Bellettre, Energy analysis of secondary droplet atomization schemes, Int. Commun. Heat Mass Tran. 117 (104666) (2020), https://doi.org/10.1016/j.icheatmasstransfer.2020.104666.